Multi-Scale Simulation of Turbulent Two-Phase Flows Induced by Injection of Fluid and Particles

V. Emelyanov[1], K. Volkov*, [2]

[1]Faculty of Power Engineering, Baltic State Technical University,
1-ya Krasnoarmeyskaya ul., 1, 190005, Saint Petersburg, Russia
[2]Engineering and Computing, Kingston University,
Friars Avenue,Roehampton Vale, SW15 3DW, London, United Kingdom

Abstract

A numerical analysis of the internal injection-driven turbulent gas-particle flow is performed to improve the current understanding and modelling capabilities of the complex flow characteristics encountered in the combustion chambers of solid rocket motors. The two-phase flow is simulated with a combined Eulerian–Lagrangian approach. The Reynolds-averaged Navier–Stokes equations and transport equations of k–ε model are solved numerically for the gas. The particulate phase is simulated through a Lagrangian deterministic and stochastic tracking models to provide particle trajectories and particle concentration. The results obtained highlight the crucial significance of the particle dispersion in turbulent flowfield and high potential of statistical methods.

Introduction

Aluminum particles in solid propellants serve two purposes: increasing specific impulse and suppressing high-frequency combustion instability. Unlike the other ingredients, aluminum particles burn in a significant portion of the combustion chamber of solid rocket motor (SRM) and produce alumina smoke and agglomerates that are carried out into the flowfield [1]. The presence of aluminum droplets in the flowfield contributes to the motor performance loss through decreasing nozzle efficiency and surface damage from droplet impingement. Detailed knowledge of particulate phase characteristics as residue size, burning time and heat release as well as particle dynamics and particle dispersion in a turbulent flowfield are essential to improve motor performance and reliability. An analysis is hampered by the complex flow features involving complex geometry, turbulence with mass injection, recirculation regions, a wide range of Mach numbers, two-phase flow phenomena, heterogeneous combustion, and uncertainties in particle density and particle size distribution.

Turbulence plays an important role in determining the wave properties through the damping effect of turbulence-induced eddy viscosity on vortical motion. Turbulence modelling becomes necessary for the evaluation of heat transfer and related phenomena (e.g. erosive burning). The interactions between organized oscillatory motions and turbulent fluctuations give rise to additional mechanisms of energy production, transfer and dissipation of wave modes. The difficulty in simulation of turbulence comes from the fact the transition is always inside the SRM, since the velocity at the head-end is equal to zero.

Aluminum droplet combustion and alumina residue behavior in the combustion chamber of SRM affect combustion instabilities by acting as driving or damping mechanisms [2]. Some of aluminum droplets remain in the motor during its operation and collect in the aft-end region. Inside the motor, these droplets are the source of slag material. Alumina slag deposition at motor aft-end results in motor performance loss, damage of thermal protection due to overheating, and possible sloshing and ejection of liquid agglomerates through the nozzle, which may cause pressure disturbances and trust imbalance.

SRMs are subject to pressure oscillations caused by vortex shedding and acoustic feedback resulting from impingement of the vortices on the nozzle and other obstacles [3–5]. The oscillatory flowfield in a SRM consists of three distinct types of wave motions: acoustic (irrotational and compressible), vortical (rotational and incompressible) and entropy (arising from unsteady heat release) modes [6]. The coupling between the acoustic wave and the incoming radial mass flow from the propellant surface generates fluctuating vorticity and causes the energy transfer from the acoustic to the vortical field (flow-turning energy losses) [3, 4]. The interactions between entropy fluctuations and non-uniform flow act as a strong source term for driving acoustic oscillations in regions with large velocity gradients [3, 7]. The three waves, along with the transient combustion response of propellant, dictate the stability behavior of SRM.

Two-phase flows with inert and burning aluminum particles as well as the influence of particles on acoustic oscillations in the combustion chamber are considered in [2,8], where the results of numerical simulations based on the Eulerian–Eulerian approach and some experimental results are reported.

Flow oscillations are expected to interact with the agglomeration process on the burning surface (mechanism 1), with the ignition and the distributed combustion that may occur in a significant portion of the combustion chamber (mechanism 2) and with alumina residues in the entire volume of the chamber (mechanism 3). The first and the third interactions are identified as damping phenomena while the second is suspected to be a driving mecha-

*Corresponding author: k.volkov@kingston.ac.uk

nism [2]. Their effectiveness depends on oscillation frequencies, droplet sizes and burning-to-residence time ratio [9]. Net contribution of aluminum to the global acoustic balance may be positive or negative [2, 3, 5].

At high frequencies, particles usually exert a damping effect on acoustic oscillations [2], and suppression of oscillations occurs due to the influence of agglomerates on the fluctuations on the burning surface (mechanism 1). At frequencies below 2000 Hz, mechanism 1 plays a minor role as compared to mechanism 3, but this interaction also leads to damping of oscillations. Some propellants that ensure stable combustion without metallic particles display a tendency to combustion instability due to addition of aluminum, which is caused by the influence of mechanism 2, which leads to enhancement of oscillations [10].

In order to extend the reliability of calculations as a predicting tool to be used for industrial applications in design and development of SRMs, one needs to improve the level of accuracy of physical models and the effectiveness of numerical schemes [11]. The study focuses on the development of numerical analysis of the internal two-phase flows with emphasis on the momentum and energy transfer between the gas and particles in presence of forced pressure oscillations, particle dynamics and particle dispersion in turbulent flowfield, interaction between turbulent and forced oscillatory flowfields, and effects of particles on steady and unsteady flow motions.

Mathematical model

The two-phase flow is simulated with combined Eulerian–Lagrangian approach. The unsteady Reynolds-averaged Navier–Stokes equations (RANS) are solved numerically for the gas phase. The particulate phase is simulated through a Lagrangian stochastic tracking model [12].

The governing equations of gas represent the conservation equations of mass, momentum and energy in Cartesian coordinates. The x axis is aligned with the centreline of the channel, and the y axis is aligned with the radius. The injection velocity, v_w, is assumed to be identical at all points of the propellant surface and to be directed normal to this surface. The parameters of the gas and particles entering the channel are assumed to be constant along the burning surface. Aluminum particles are injected from the surface of the channel at points uniformly distributed over the channel length.

In Cartesian coordinates (x, y, z), an unsteady 3D flow is described by the following equations (for simplicity, chemical reactions are not included)

$$\frac{\partial \rho}{\partial t} + \nabla \cdot (\rho \boldsymbol{v}) = 0; \tag{1}$$

$$\frac{\partial \rho \boldsymbol{v}}{\partial t} + \nabla \cdot (\rho \boldsymbol{v}\boldsymbol{v}) = -\nabla p + \nabla \cdot \tau - \sum_i \boldsymbol{F}_{\mathrm{p}i} n_{\mathrm{p}i}; \tag{2}$$

$$\frac{\partial \rho e}{\partial t} + \nabla \cdot [(\rho e + p)\, \boldsymbol{v}] = -\nabla \cdot \boldsymbol{q} + \nabla \cdot (\tau \cdot \boldsymbol{v}) - \\ - \sum_i W_{\mathrm{p}i} n_{\mathrm{p}i} - \sum_i Q_{\mathrm{p}i} n_{\mathrm{p}i}. \tag{3}$$

The equation of state of an ideal gas is

$$p = (\gamma - 1)\rho \left[e - \frac{1}{2} \left(v_x^2 + v_y^2 + v_z^2 \right) \right].$$

Here, t is the time, ρ is the density, v_x, v_y, and v_z are the velocity components in the coordinate directions x, y and z, p is the pressure, e is the total energy per unit mass, T is the temperature, and γ is the specific heat capacity ratio. The subscript p corresponds to the particles. Summation is performed over all particles of the ith fraction.

The viscous stress tensor and the heat flux vector are related to the velocity and temperature fields by the relations

$$\tau = \mu_e \left[\nabla \boldsymbol{v} + (\nabla \boldsymbol{v})^* \right], \quad \boldsymbol{q} = -\lambda_e \nabla T,$$

where μ_e is the effective viscosity and λ is the effective thermal conductivity. The adjoint tensor is indicated by the asterisk.

The equations (1)–(3) are suitable for both laminar and turbulent flows. For turbulent flow, the effective viscosity, μ_e, is calculated as the sum of molecular viscosity, μ, and turbulent eddy viscosity, μ_t, and the effective thermal conductivity, λ_e, is expressed in terms of effective viscosity and Prandtl number

$$\mu_e = \mu + \mu_t, \quad \lambda_e = c_p \left(\frac{\mu}{\mathrm{Pr}} + \frac{\mu_t}{\mathrm{Pr}_t} \right),$$

where c_p is the specific heat capacity at constant pressure, and $\mathrm{Pr} = 0.72$ and $\mathrm{Pr}_t = 0.9$. The eddy viscosity is calculated by the Kolmogorov–Prandtl relationship ($\mu_t = c_\mu \rho k^2/\varepsilon$).

The transport equations of the turbulent kinetic energy, k, and its dissipation rate, ε, are written in the form

$$\frac{\partial \rho k}{\partial t} + (\rho \boldsymbol{v} \cdot \nabla)\, k = \nabla \left[\left(\mu + \frac{\mu_t}{\sigma_k} \right) \nabla k \right] + \\ + P - \rho\varepsilon + E_{\mathrm{p}}; \tag{4}$$

$$\frac{\partial \rho \varepsilon}{\partial t} + (\rho \boldsymbol{v} \cdot \nabla)\, \varepsilon = \nabla \left[\left(\mu + \frac{\mu_t}{\sigma_\varepsilon} \right) \nabla \varepsilon \right] + \\ + \frac{\varepsilon}{k} \Big(c_{\varepsilon 1} P - c_{\varepsilon 2} \rho \varepsilon \Big) + \Phi_{\mathrm{p}}. \tag{5}$$

Here, P is the turbulent generation term. The Kato–Launder correction to the turbulence generation term is applied

$$P = \mu_t |S|^{1/2} |\Omega|^{1/2}.$$

The invariants of the strain rate tensor and the rotation rate tensor are found from the relations

$$|S| = (2 S_{ij} S_{ij})^{1/2}, \quad |\Omega| = (2 \Omega_{ij} \Omega_{ij})^{1/2},$$

where

$$S_{ij} = \frac{1}{2} \left(\frac{\partial v_i}{\partial x_j} + \frac{\partial v_j}{\partial x_i} \right), \quad \Omega_{ij} = \frac{1}{2} \left(\frac{\partial v_i}{\partial x_j} - \frac{\partial v_j}{\partial x_i} \right).$$

The source terms in the right hand sides of equations (2) and (3) take into account the exchange of momentum

between the phases, the heat transfer between the gas and the particles, and the work done by the particles on gas. The intensities of momentum and energy exchange between the phases are determined as the product of the number concentration of the particles and the intensity of interphase exchange per one particle ($n_{\mathrm{p}i}$ is the concentration of the particles of the ith fraction per unit volume). The work done by the particles on gas is calculated as $W_{\mathrm{p}} = \boldsymbol{F}_{\mathrm{p}} \cdot \boldsymbol{v}_{\mathrm{p}}$.

The source terms E_{p} and Φ_{p} in the equations of k–ε model (4) and (5) take into account the effect of particulate phase on turbulence (turbulence modulation).

It is assumed that flow unsteadiness caused by external pressure oscillations exerts a minor effect on the flow core [13, 14]. For modelling the flow core, equations (4) and (5) are used. The model constants are assigned the following values: $c_\mu = 0.09$, $\sigma_k = 1.0$, $\sigma_\varepsilon = 1.3$, $c_{\varepsilon 1} = 1.44$, $c_{\varepsilon 2} = 1.92$. Near the wall (in the internal region of the boundary layer), the k–l turbulence model is used. The turbulent kinetic energy is found from equation (4). The dissipation rate is calculated by using an algebraic dependence with allowance for the influence of flow unsteadiness on the turbulence scale [15], rather than by means of numerical integration of equation (5).

The particles are simulated through a Lagrangian deterministic or stochastic tracking models to provide particle trajectories [12]. The virtual mass and Basset forces due to their small magnitudes, and the Magnus force due to lack of knowledge about particle angular momentum are neglected. The resulting force acting on a particle is the drag force. The equations describing translational motion and convective heat transfer of a spherical particle in a turbulent flowfield are written in the form

$$\frac{d\boldsymbol{r}_{\mathrm{p}}}{dt} = \boldsymbol{v}_{\mathrm{p}}; \tag{6}$$

$$\frac{d\boldsymbol{v}_{\mathrm{p}}}{dt} = \frac{3C_{\mathrm{D}}\rho}{8\rho_{\mathrm{p}} r_{\mathrm{p}}} \left|\boldsymbol{v} - \boldsymbol{v}_{\mathrm{p}}\right| \left(\boldsymbol{v} - \boldsymbol{v}_{\mathrm{p}}\right); \tag{7}$$

$$c_{\mathrm{p}}^{m} m_{\mathrm{p}} \frac{dT_{\mathrm{p}}}{dt} = 2\pi r_{\mathrm{p}} \mathrm{Nu}_{\mathrm{p}} \lambda \left(T - T_{\mathrm{p}}\right); \tag{8}$$

$$\frac{dm_{\mathrm{p}}}{dt} = \dot{m}_{\mathrm{p}}.. \tag{9}$$

To calculate the drag coefficient and the Nusselt number. solution of micro-level problem is used [1].

The fluid velocity in equation (7) represents a random function of the Cartesian coordinates and time. The fluid velocity is a sum of the averaged velocity, $\langle \boldsymbol{v} \rangle$, and the random velocity, $\boldsymbol{v}'$. The averaged velocity is found from the solution of RANS equations (1)–(3). The turbulence is taken into account by introducing random velocity fluctuations into equation (7). The particles are assumed to interact with a succession of turbulence eddies, as they move through the computational domain [12]. The duration of interaction between an eddy and a particle is determined as the smaller one between the eddy life-time and the transit time required for a particle to transverse the eddy.

Equations (6)–(9) are integrated along the path of an individual particle and require specification of the initial conditions — the Cartesian coordinates, velocity, temperature and mass of a particle at the time $t = 0$ (on the injection surface).

Numerical method

The calculations are performed with the in-house CFD code developed for aerospace and related applications. The details of the code are described in [16].

Flow solution is provided using cell-centered finite volume formulation of unsteady 3D compressible RANS equations on unstructured meshes. Governing equations are solved by the firth step Runge–Kutta time marching scheme. Piecewise parabolic method (PPM) is applied to inviscid fluxes, and central difference scheme of the second order is applied to viscous fluxes. For the injection-driven flows, the fluid velocity in the bulk of the computational domain is much smaller than the acoustic speed. The conventional numerical algorithms developed for compressible flows encounter disparity of eigenvalues of the Jacobian and singular behavior of the pressure gradient in the momentum equation. Block-Jacobi preconditioning technique and dual time-stepping integration scheme are employed to stabilize calculations. The numerical scheme is efficient and robust over a wide range of Mach numbers.

To solve the Cauchy problem for particle equations, the fourth-order Runge–Kutta method and methods that permit resolving in the solution rapidly and slowly decaying components are used. To supply fluid parameters at points lying in the particle trajectory, the bi-linear interpolation method is employed. The integration time step along each trajectory is limited to the time and space turbulence scales. In the calculations, from 10^3 to 10^5 trajectories of sample particles depending on their size are modelled.

The unsteady calculations are performed in the following manner. After convergence toward a steady state solution, the channel flow is excited close to its first longitudinal mode by means of one period of head-end forcing. Pressure oscillations equal to 5% of the head-end mean pressure at imposed acoustic frequencies are forced at the head-end in order to analyze unsteady flowfield. Then, the response of the flowfield to that perturbations is analyzed in terms of frequency and exponential damping.

Geometry and mesh

The physical model consists of axisymmetric channel with a closed head-end. Length of channel is $L = 1.88$ m, and its radius is $h = 0.2$ m. The pre-mixed gas and aluminum particles are uniformly injected from the channel walls to simulate the evolution of combustion products of solid propellant.

The air flow rate is 20 kg/(m·s) that corresponds to the propellant burning rate of 10 mm/s and density of 2296 kg/m^3. The Mach numbers based on the surface injec-

tion velocity is about 0.002. Periodic pressure oscillations with an amplitude of 5% of the mean pressure are imposed at the channel head-end to generate longitudinal standing acoustic waves in the computational domain. On the injection wall ($r = h$), the velocities of the gas and particulate phase are subjected to the normal injection conditions ($u = u_{\rm p} = 0$, $v = v_{\rm p} = -\varphi v_{\rm w}$, where φ takes into account initial dynamic non-equilibrium of the phases, $\varphi = 0.01$). No-slip and no-penetration boundary conditions are applied to the solid wall. The temperature of the wall is fixed. Non-reflecting boundary conditions are applied to the channel outlet to allow for traveling acoustic waves in the channel.

A limited number of injection points located on the channel surface are considered. The particles are distributed following a uniform law. Three different particle diameters are considered (10, 20 and 100 μm).

The computational mesh consists of 400 nodes in the axial direction, and 100 nodes in the radial direction. The mesh nodes are clustered near the injection surface to resolve the vortical wave structure and turbulent boundary layer. The smallest mesh step size near the channel walls corresponds to $y^+ \sim 5$, and each vortical wavelength is covered by 10 nodes.

Results and discussion

In the unsteady case, the flow structure near the wall is complicated and testifies to the presence of an acoustic boundary layer inside which there are velocity fluctuations induced by propagation of unsteady shear waves (vorticity waves) [3,5]. Vorticity perturbations are formed due to injection from the surface owing to the no-slip conditions on the wall, propagate inward the channel, and are damped by viscous effects. In the flow core, there is 1D distribution of the axial velocity fluctuations, which is accurately described by the existing linear theory [3]. The influence of viscosity on propagation of vorticity waves is proportional to the frequency of oscillations. Flow turbulence leads to more appreciable damping of the amplitude of the axial velocity fluctuations because of additional generation of eddy viscosity.

The overall flow development is described by three distinct regimes as shown in the Figure 1: laminar (region 1), transitional (region 2) and turbulent (region 3). Viscous effects play an important role in the vicinity of the head-end ($0 < x/h < 1/\mathrm{Re}$). The flow is predominantly laminar in the upstream part of the channel ($0 < x/h < 5$) and undergoes transitions to turbulence as a result of hydrodynamic instability ($5 < x/h < 10$). Unlike channel flow with solid walls, the outbreak of turbulence occurs away from the walls (shaded region). The peak of turbulence intensity moves closer to the wall in the downstream direction until the surface injection prohibits further penetration of turbulence ($10 < x/h < 60$). As the flow develops farther downstream, the profile of axial velocity becomes much steeper near the wall, but flatter in the core region (near the centreline).

Profiles of axial velocity predicted with the developed

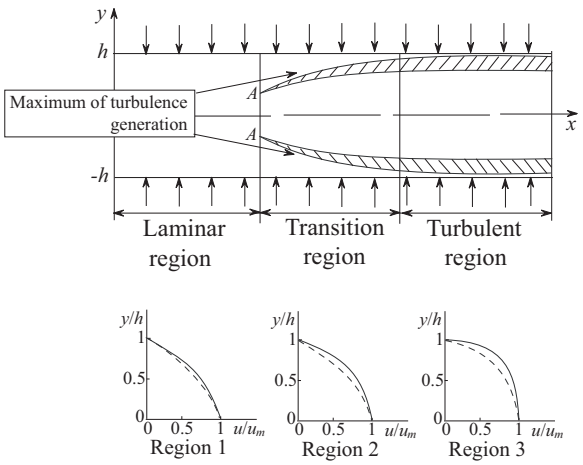

Figure 1. Flow regimes in channel with fluid injection

model (solid lines) more flatter in the core region and more steeper in the near wall region than those in vortical flow (dashed lines). The profiles of radial velocity predicted with RANS and model of vortical flow are in a good agreement. Compressibility effects in the downstream part of the channel lead to small discrepancy of the results based on different models. Reynolds number has a small influence on profiles of axial and radial velocities in channel formed by wall injection.

A negative pressure gradient due to flow acceleration exists in the injection-driven flow, which exerts an appreciable effect on the mechanism and intensity of turbulent transfer. Laminar to turbulent transition occurs further downstream (except for the near-wall and near-centreline regions), which is manifested in the presence of a turbulence front and displacement of the turbulent kinetic energy peak from the wall inward the flow. Near the channel wall, there is a layer with a low (tending to zero) of the turbulent kinetic energy (displacement zone). Near the injection wall and the channel centreline, the flow is virtually laminar. An increase in the level of turbulent velocity oscillations is observed in the strong shear region at a certain distance from the channel wall, where the fluid particles moving normal to the surface change the direction of their motion to the opposite one in a narrow subsurface layer.

Acoustic oscillations exert significant influence on unsteady flow evolution. In particular, single-harmonic oscillations excite a fluctuating flow with a broadband frequency spectrum [3] (this phenomenon is referred to as acoustically induced turbulent motion). Generation of turbulence by organized external forcing is viewed as an energy transfer process from the acoustic flowfield to the turbulent flowfield. The coupling between the Reynolds stresses and the gradient of acoustic velocity provides a mechanism to transfer the kinetic energy from acoustic motions to turbulent fluctuations. Furthermore, an early transition from laminar regime to turbulent one occurs depending on the forcing amplitude and frequency (Figure 1). The effect of energy exchange tends to be more

profound for low-frequency acoustic oscillations.

The radial profiles of time-averaged axial velocity and turbulent kinetic energy at various axial locations (solid lines) are shown in the Figure 2 and Figure 3 for the first longitudinal mode ($f \sim 1000$ Hz, $\phi = 0.02$). Lines 1 correspond to the simulation of the injection-driven flow based on RANS equations and k–ε model, and lines 2 correspond to large-eddy simulation of channel flow induced by wall injection [16]. The profiles corresponding to steady state flow (dashed lines) are also included for comparison. An enhanced level of turbulence due to acoustic excitation is clearly observed. The acoustic waves induce flow instability and cause transfer of energy from the oscillatory organized to the turbulent field.

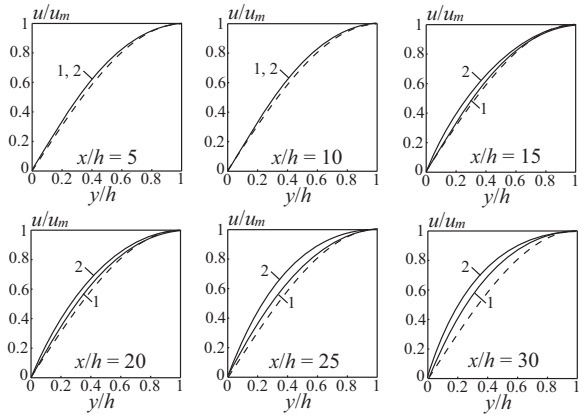

Figure 2. Radial profiles of axial velocity

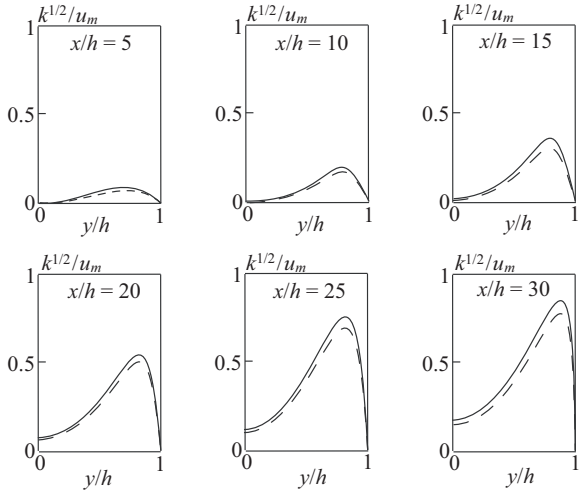

Figure 3. Radial profiles of turbulent kinetic energy

As the ratio of the particle relaxation time to the acoustic time for fine particles is comparatively small (Stk $\rightarrow$ 0), they respond to the turbulent oscillations of the carrier flow velocity and, therefore, to changes in its parameters and follow the acoustic velocity fluctuations. Coarse particles (Stk $\rightarrow \infty$) do not respond to the turbulent oscillations of the fluid flow velocity.

Particle trajectories are computed for different particle diameters. A difference exists between particle trajectories calculated from laminar and turbulent flow fields. Small particles deviate from their mean flow paths under the influence of gas flow oscillations and turbulent dispersion, and enhance interphase interactions. The dispersion of particles is controlled by the particle Stokes number. Limiting trajectory of particles where concentration of particles increases is clearly observed in the calculations (Figure 4). Dispersion of particles leads to increasing the particles residence time in the channel. The particle damping effect is defined by the particle loading and the ratio of particle relaxation time to turbulent time scale. The particles lead to damping of turbulent fluctuations and have laminarisation effect resulting in additional dissipation of turbulent kinetic energy due to relative motion of gas and particles. The turbulence modulation effect is more visible for small particles.

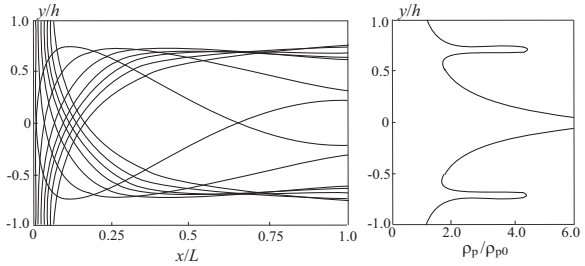

Figure 4. Particle trajectories and particle mass concentration at $d_{\rm p} = 20$ μm

Figure 5 presents the trajectories of aluminum oxide particles ($r_{\rm p} = 5$–50 μm) in an injection-driven flow ($v_w = 5$ m/s, $u_{{\rm p}w} = 0$ and $v_{{\rm p}w} = v_w$). The influence of the sluggishness of a particle on its scattering is inconclusive, since particles of different masses execute motion in different regions with a different turbulence intensity. The influence of velocity fluctuations on the particle motion is manifest when the particle gets into the turbulent region of the flow. A non-monotonic change in the turbulent kinetic energy along the axial coordinate leads to a non-monotonic change in the degree of particle involvement in the fluid flow, which is determined by the relation between the particle relaxation time and the turbulent time scale.

For large particles, velocity fluctuations produce no significant effect on the impurity motion throughout the region of flow development because of the inertia of such particles. Weak migration of particles towards decreasing turbulent kinetic energy is observed only for particles injected into the channel at a considerable distance from its head-end (at $x_{\rm p0} > 9$). Small particles are scattered rather strongly.

The oscillatory velocity field is split into acoustic and vortical flow motions. Several two-phase flow simulations are carried out to study the effects of the particle Stokes number on the oscillations behavior.

The Figure 6a shows the radial profiles of amplitude of axial velocity fluctuations ($f \sim 3770$ Hz, $\phi = 0.02$) at the mid-section of channel ($x/L \sim 0.5$) where flow is turbulent. The influence of large particles on the acous-

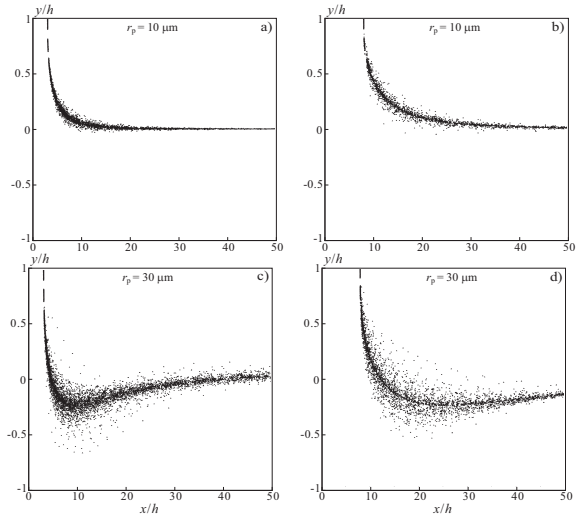

Figure 5. Trajectories of sample particles in the channel at $v_w = 5$ m/s

tic velocity is negligible because of their high inertia, and small particles effectively reduce the velocity oscillations. Turbulence exerts a small influence on the acoustic wave structure. Its primary contribution lies in the dissipation of the vortical motion through the turbulence-enhanced eddy viscosity. The Figure 6b shows results of the first longitudinal mode oscillations ($f \sim 943$ Hz, $\phi = 0.02$). The damping effect of particles on the vortical flow motion is observed. An optimum size of particles corresponding to acoustic Stokes number close to unity is obtained to exert the maximum dissipation on flow oscillations.

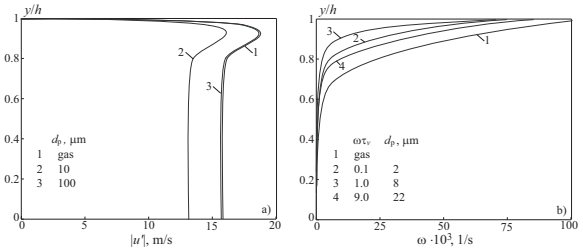

Figure 6. Effect of particles on acoustic and vortical flow fields at $m_p = 0.2$

Figure 7 shows the radial profiles of the amplitude of axial velocity fluctuations in a laminar flow at a point located approximately in the middle of the channel ($x/L = 0.5$) for $f = 1885$ Hz and $\phi = 0.02$. The flow is laminar, the mass fraction of particles is assumed to be $m_p = 0.2$, and the initial particle velocity is 0.1 m/s, which approximately corresponds to 10% of the injection velocity.

There are two characteristic flow regions. In the near-wall region of the flow ($y/h > 0.6$), there are significant oscillations of acoustic velocity and vorticity. In the axial region ($y/h < 0.6$), the vorticity waves decay because of viscous dissipation, and the influence of acoustic effects starts to dominate. The presence of particles leads to suppression of acoustic velocity fluctuations owing to

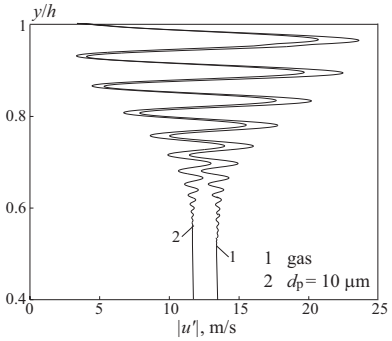

Figure 7. Radial profiles of the amplitude of axial velocity fluctuations

momentum and energy exchange with the gas. The overall effect of the particulate phase is determined by the particle loading, dynamic and thermal particle relaxation times, and frequency of acoustic oscillations. Fine particles exert a significant effect on the acoustic flowfield, rapidly reaching equilibrium with the gas and effectively changing the density of the mixture, whereas coarse particles exert a minor effect. The maximum amplitude of axial velocity fluctuations is $|u'|_{\max} = 13.2$ m/s for $d_p = 10$ μm and $|u'|_{\max} = 15.5$ m/s for $d_p = 100$ μm (this value coincides with the corresponding value in the pure gas).

Heat release as a result of bi-molecular chemical reaction in the gas phase has a significant impact on radial velocity profiles. The RANS calculations indicate universal profile of radial velocity compared to LES calculations (Figure 8). Dashed line corresponds to the theoretical solution [7].

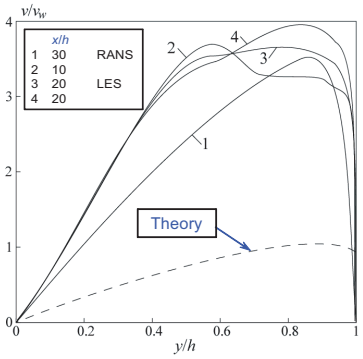

Figure 8. Radial velocity profiles prediction with RANS (line 1) and LES (lines 2–4)

Chemical reactions insignificantly influence the profile of axial velocity but have significant influence on the profiles of radial velocity (Figure 9). The radial velocities of gas and particulate phases increase in the near-wall region where the chemical reactions take place. Diameter of particles is 10 μm. Bullets correspond to the theoretical solution [7].

Conclusions

A numerical simulation of internal injection-driven turbulent gas-particle flow is performed with forced pressure oscillations. Flow unsteadiness is induced by forced

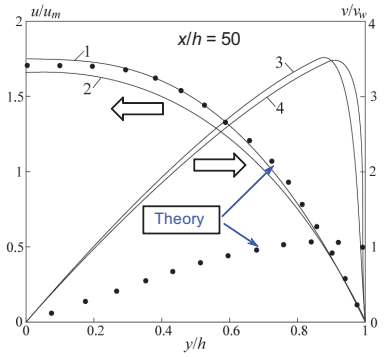

Figure 9. Axial and radial velocities profiles of gas (lines 1 and 3) and particles (lines 2 and 4)

periodic pressure oscillations at the channel head-end. The gas is simulated solving the RANS equations and equations of k–ε turbulence model, and the particulate phase is treated with a Lagrangian model. The results obtained highlight the crucial significance of the particle dispersion in turbulent flowfield and high potential of statistical methods. Strong coupling between acoustic oscillations, vortical motion, turbulent fluctuations and particle dynamics is observed.

Particle trajectories are computed to assess the effects of the turbulent flowfield on the slag dispersion for different particle diameters. Turbulent dispersion is mainly observed for small particles. Dispersion of particles leads to increasing particle residence time and changes combustion efficiency. The ratio of particle relaxation time to acoustic characteristics time plays an important role in dictating the two-phase flow interactions with oscillatory internal flow. A maximum attenuation of acoustic waves occurs when those times are comparable. Small particles exert greater influence on the dispersion of acoustic wave through its effective modification of mixture compressibility.

Acoustic oscillations provide additional mechanism to energy transfer from periodic motion to turbulence leading to an enhanced level of turbulence and an early transition from laminar to turbulence. On the other hand, eddy viscosity tends to suppress vortical flow motion caused by acoustic waves. Fine particles (equilibrium flow) exert the most pronounced damping effect at high frequencies of oscillations. For coarse particles, which are not involved into the wave motion (frozen flow), momentum and heat exchange with the gas is negligibly small, and the effect of particles on acoustic oscillations in the channel is not observed.

References

1. K.N. Volkov, Combustion of single aluminium droplet in two-phase flow, *Heterogeneous Combustion*, Nova Science, 2011, pp. 191–260.
2. J. Dupays, Two-phase unsteady flow in solid rocket motors. *Aerospace Science and Technology*, 2002, 6(6), pp. 413–422.
3. G.A. Flandro, Effects of vorticity on rocket combustion stability, *Journal of Propulsion and Power*, 1995, 11(4), pp. 607–625.
4. F. Vuillot, Vortex-shedding phenomena in solid rocket motors, *Journal of Propulsion and Power*, 1995, 11(4), pp. 626–639.
5. S.V. Apte, V. Yang, Unsteady flow evolution and combustion dynamics of homogeneous solid propellant in a rocket motor, *Combustion and Flame*, 2002, 131(1–2), pp. 110–131.
6. W. Cai, F. Ma, V. Yang, Two-phase vorticoacoustic flow interactions in solid-propellant rocket motors, *Journal of Propulsion and Power*, 2003, 19(3), pp. 385–396.
7. F.E.C. Culick, The stability of one-dimensional motions in a rocket motor, *Combustion Science and Technology*, 1973, 7(4), pp. 165–175.
8. J. Dupays, F. Vuillot, Propagation of acoustic waves in a two-phase vaporizing mixture, *Journal of Propulsion and Power*, 2002, 18(1), pp. 222–224.
9. S.Temkin, Attenuation and dispersion of sound in dilute suspensions of spherical particles, *Journal of Acoustical Society of America*, 2000, 108(1), pp. 126–146.
10. K.P. Brooks, M.W. Beckstead, Dynamics of aluminum combustion, *Journal of Propulsion and Power*, 1995, 11(4), pp. 769–780.
11. V.N. Emelyanov, I.V. Teterina, K.N. Volkov, Simulation of turbulent two-phase flows in the combustion chambers of solid rocket motors, *Proceedings of the 5th European Conference for Aeronautics and Space Sciences, 1–5 July 2013, Munich, Germany*, 2013, pp. 1–15.
12. K. Volkov, Internal turbulent two-phase flows formed by wall injection of fluid and particles, *5th ECCOMAS Computational Fluid Dynamics Conference, 14–17 June 2010, Lisbon, Portugal*, 2010, 01649.
13. J. Cousteix, A. Desopper, R. Houdeville, Structure and development of a turbulent boundary layer in an oscillating external flow, *First International Symposium on Turbulent Shear Flows, 18–20 April 1977, Pennsylvania State University, Pennsylvania, USA*, 1977, pp. 154–171.
14. B.R. Ramaprian, S.W. Tu, An experimental study of oscillatory pipe flow at transitional Reynolds numbers, *Journal of Fluid Mechanics*, 1980, 100(3), pp. 513–544.
15. I.-S. Tseng, V. Yang, Combustion of a double-base homogeneous propellant in a rocket motor, *Combustion and Flame*, 1994, 96(4), pp. 325–342.
16. K.N. Volkov, Large-eddy simulation of free shear and wall-bounded turbulent flows, *Atmospheric Turbulence, Meteorological Modelling and Aerodynamics*, USA, Nova Science, 2010, pp. 505–574.